Author Manuscript

Author Manuscript

Author Manuscript

Author Manuscript

HHS Public Access

Author manuscript

Phys Med Biol. Author manuscript; available in PMC 2024 January 23.

Published in final edited form as:

Phys Med Biol. ; 68(3): . doi:10.1088/1361-6560/acae16.

Markerless Motion Tracking with Simultaneous MV and kV Imaging in Spine SBRT Treatment – a Feasibility Study

Weixing Cai,

Qiyong Fan,

Feifei Li,

Xiuxiu He,

Pengpeng Zhang,

Laura Cervino,

Xiang Li,

Tianfang Li

Memorial Sloan Kettering Cancer Center, Department of Medical Physics, 1275 York Avenue, New York, NY 10065

Abstract

Objective: Motion tracking with simultaneous MV-kV imaging has distinct advantages over single kV systems. This research is a feasibility study of utilizing this technique for spine SBRT through phantom and patient studies.

Approach: A clinical spine SBRT plan was developed using 6xFFF beams and nine sliding-window IMRT fields. The plan was delivered to a chest phantom on a linear accelerator. Simultaneous MV-kV image pairs were acquired during beam delivery. KV images were triggered at predefined intervals, and synthetic MV images showing enlarged MLC apertures were created by combining multiple raw MV frames with corrections for scattering and intensity variation. DRR templates were generated using high-resolution CBCT reconstructions (isotropic voxel size $(0.243mm)^3$) as the reference for 2D-2D matching. 3D shifts were calculated from triangulation of kV-to-DRR and MV-to-DRR registrations. To evaluate tracking accuracy, detected shifts were compared to known phantom shifts as introduced before treatment. The patient study included a T-spine patient and an L-spine patient. Patient datasets were retrospectively analyzed to demonstrate the performance in clinical settings.

Main Results: The treatment plan was delivered to the phantom in five scenarios: no shift, 2mm shift in one of the longitudinal, lateral and vertical directions, and 2mm shift in all the three directions. The calculated 3D shifts agreed well with the actual couch shifts, and overall, the uncertainty of 3D detection is estimated to be 0.3mm. The patient study revealed that with clinical patient image quality, the calculated 3D motion agreed with the post-treatment cone beam CT. It is feasible to automate both kV-to-DRR and MV-to-DRR registrations using a mutual information-based method, and the difference from manual registration is generally less than 0.3mm.

Author Manuscript Author Manuscript Author Manuscript Author Manuscript

Significance: The MV-kV imaging-based markerless motion tracking technique was validated through a feasibility study. It is a step forward toward effective motion tracking and accurate delivery for spinal SBRT.

1. Introduction

Studies have shown excellent local control in stereotactic body radiotherapy (SBRT) for treating spinal metastases (Greco *et al* 2015, Zeng *et al* 2019). Due to the high ablative dose (8 to 24Gy per fraction) and proximity to the spinal cord, it is critical to ensure that the spinal SBRT is delivered to targets with high accuracy and precision (Greco *et al* 2015, Zeng *et al* 2019, Vellayappan *et al* 2018, Saenz *et al* 2019). As the patient's involuntary motion during treatment is a major issue that adversely impacts the precision of beam delivery, an accurate and effective motion tracking technique is highly desired for successful treatments (Hall *et al* 2011, Keall *et al* 2018). While markerless tracking has been reported for lung SBRT (Rozario *et al* 2018, Shieh C *et al* 2015, van Sornsen *et al* 2015, de Bruin *et al* 2021) and liver SBRT (Nankali *et al* 2018) using either kV or MV images, this work was focused on the application of simultaneous MV and KV images for spinal SBRT.

To address the challenges with spinal SBRT, kV image-based motion tracking techniques have been developed over the past decades (Bertholet *et al* 2019, Kim *et al* 2018a and 2018b, Roggen *et al* 2020, Kaur *et al* 2019, Graeper *et al* 2021, Ho *et al* 2007, Furweger *et al* 2011, Jin *et al* 2008, Montgomery *et al* 2017, Gurney-Champion *et al* 2013, Verbakel *et al* 2015). For examples, the X-sight spine tracking system on the CyberKnife platform (Accuray Inc, Sunnyvale, CA) and the ExacTrac system (BrainLAB AG, Feldkirchen, Germany), both employ kV image pairs for quantitative motion tracking (Ho *et al* 2007, Furweger *et al* 2011, Jin *et al* 2008, Montgomery *et al* 2017). Nevertheless, these systems require either a dedicated machine or additional equipment beyond the standard linear accelerators. A more cost-effective and convenient solution on conventional linear accelerator platform would be to utilize the readily available on-board imaging systems (OBI) for motion monitoring. Varian (Varian Medical Systems, Palo Alto, CA), for example, provides a tool called Intrafraction Motion Review (IMR) on their TrueBeam platform, which offers on-treatment kV imaging for motion monitoring at certain trigger conditions defined by the user. However, this method does not provide quantitative information about patient motion and relies solely on user's visual judgement to make clinical decisions, which is therefore prone to human errors (Bertholet *et al* 2019, Kim *et al* 2018a and 2018b, Roggen *et al* 2020, Kaur *et al* 2019, Graeper *et al* 2021).

To broaden the application of KV image-based motion tracking in the conventional linear accelerator platform, researchers have also developed methods to provide quantitative 3D motion information by analyzing kV images acquired from multiple gantry angles during RT (Roggen *et al* 2020, Kaur *et al* 2019, Graeper *et al* 2021, de Bruin et al 2021 and Hazelaar et al 2018). While these methods are capable of detecting submillimeter motions with good quality kV images, the issues with these methods of using kV imaging only, as pointed out by the authors, are: 1) the accuracy of detecting movements along the direction parallel to the kV beam is low (Graeper *et al* 2021); 2) image quality degraded significantly at some gantry angles due to excessive attenuation (Kaur *et al* 2019). To overcome these issues,

Author Manuscript Author Manuscript Author Manuscript Author Manuscript

we propose to combine kV imaging with simultaneous MV imaging for more effective motion tracking, referred to as MV-kV imaging hereafter. The advantages of including MV imaging for motion tracking are: 1) the stronger penetration power of the MV beam can sometimes generate better image quality than kV imaging beam at gantry angles where x-ray attenuation is heavy; 2) when the kV beam suffers from high attenuation in the patient's lateral direction, the 90-degree apart MV beam is at the anterior-posterior direction and can have better signal for motion detection; 3) Motion detected from MV beam's eye view has more dosimetry impact than that detected from KV beam's eye view (Yue 2011, et al Mishra et al 2014, and Bryant et al 2014); 4) Simultaneously acquired MV-kV image pairs make it possible to calculate 6D motions in real-time (Hunt et al 2016, Crotteau et al 2022). Clinical experiences with simultaneous MV-kV imaging showed distinct advantages over single kV imaging system in detecting fiducial motions in three dimensions in real-time for prostate SBRT (Zhang *et al* 2016, Gorovets *et al* 2020, Happersett *et al* 2019, Hunt *et al* 2016, Crotteau *et al* 2022). This work aims to investigate the use of MV-kV imaging for markerless motion monitoring in spine SBRT without invasive fiducials.

2. Materials and Methods

2.1. Spinal SBRT Plan and MV-kV Image Acquisition

Figure 1 illustrates a typical field arrangement of the clinical spinal SBRT plan transferred to an anthropomorphic phantom called 'LUNGMAN' (Kyoto Kagaku Co., Japan). The plan was constructed using nine sliding-window IMRT fields from posterior and lateral angles. An automated planning process named Expedited Constrained Hierarchical Optimization (ECHO) (Zarepisheh *et al* 2019) was used to optimize the plan. All fields were highly modulated 6xFFF beams to produce fast dose fall-off. The phantom has a physical dimension of 43cm × 40cm × 48cm and a weight of 18 kilograms, comprising of synthetic bones made of epoxy resin and soft tissues made of polyurethane. The planning target was the 8^{th} thoracic vertebral body with a prescription dose of 2700cGy in three fractions.

The plan was delivered on a Varian TrueBeam linear accelerator (Varian Medical Systems, Palo Alto, CA) with console software version v2.7, and kV and MV images were automatically acquired during plan delivery with Varian's proprietary software iTools Capture. The kV imager (model 4030CB) has a physical dimension of 40 cm × 30 cm with an image matrix of 1024 × 768 and a pixel size of 0.388 mm. The MV panel (model AS1200) has a physical dimension of 43cm × 43cm with an image matrix of 1280 × 1280 and a pixel size of 0.336 mm. Given a source-to-imager distance (SID) of 150 cm and a source-to-axis distance (SAD) of 100cm, the effective pixel sizes at the isocenter are 0.259 mm and 0.224 mm, respectively, for the KV and MV images. The MV images were continuously acquired with a frame rate of 11.4 fps, while the KV images were triggered at every 500 MU during radiation delivery. Both MV and kV images were acquired with dark-field corrections and flood-field corrections.

2.2 High-resolution DRRs as matching templates

Motion tracking was achieved by registering on-treatment MV and KV images to our customized digitally reconstructed radiograph (DRR) templates. To improve the accuracy

Author Manuscript Author Manuscript Author Manuscript Author Manuscript

of registration, high-resolution spine-only DRR templates were created from retrospectively reconstructed CBCT reconstructions with an isotropic voxel size of $(0.243\ \text{mm})^3$. The high resolution CBCT was obtained by sending acquired raw projections to a Varian proprietary software program (namely iTools Reconstruction) to compute a CBCT volume with a customizable voxel size and the same reconstruction algorithm as used in clinic. On a stand-alone workstation (Intel Xeon CPU@2.1GHz, 32GB DDR, 64-bit Windows 10), a CBCT reconstruction with matrix size of 1024×1024×700 takes less than 4 minutes on CPU, which can be further reduced with GPU implementation and should not delay clinical workflow. The orientation of the high-resolution CBCT was corrected by CBCT to planning CT registration to match the actual treatment position. An in-house software using detector pixel-driven forward projection algorithm was employed for the DRR template calculations for all planned MV-beam angles and KV-beam angles. Figure 2 shows three spine-only DRR templates generated with CBCT voxel sizes of $0.243\times0.243\times0.243\ \text{mm}^3$, $1\times1\times1\ \text{mm}^3$, and $1\times1\times2\ \text{mm}^3$, respectively. Higher-resolution DRRs have clearly sharper edges thus leading to less uncertainty for image matching.

2.3 MV image preprocessing

During the treatment delivery, about 400 to 500 frames of raw MV images were collected for each gantry angle. However, as the sliding-window IMRT technique utilizes a set of small MLC apertures, it is not always possible to visualize useful landmarks in a single MV frame for reliable image matching. To solve this issue, an enhanced synthetic treatment beam (ESTB) imaging technique was used (Li *et al* 2021). The main idea of this technique is to combine multiple continuous MV frames, after scatter reduction and beam intensity variation corrections, to generate a synthetic MV image with enlarged field of view (FOV). Depending on the plan and patient anatomy, combining 50 to 100 consecutive frames is usually sufficient to produce synthetic MV images with reasonable FOV sizes for matching on spine structures. The frame combining process had an inherent time delay of 5–10 seconds, which was deemed acceptable for spine motion detection because the motions were typically not continuous but random spontaneous bulk motions.

2.4 Motion tracking

To determine 3D motion, a pair of a synthetic MV image and an on-treatment kV image were firstly registered to their respective DRR templates separately for 2D matching. The 2D results were then used to triangulate the 3D shift. To demonstrate feasibility of the technique and to ensure matching accuracy, MV-to-DRR and kV-to-DRR registrations were performed manually for each beam. An automatic registration approach using mutual information (MI) was also evaluated with the region of interest (ROI) selected as projected PTV contour plus 1 cm margin. Figure 3 shows the coordinate system of simultaneous MV and kV image acquisition on a linear accelerator gantry system. Both MV and kV images were scaled to isocenter. From MV-to-DRR registration, we have

$$\begin{cases} q_{MV} = dz \\ p_{MV} = -dx \cdot \sin(G_{MV} - 90) + dy \cdot \cos(G_{MV} - 90) \end{cases} \quad (1)$$

Author Manuscript Author Manuscript Author Manuscript Author Manuscript

where q_{MV} and P_{MV} are shifts in the vertical and horizontal direction, respectively, on the MV imaging plane, and dx, dy, and dz are 3D shifts in the patient's coordinate system in lateral (left +), vertical (posterior +) and longitudinal (superior +) directions. Image acquisition angle G_{MV} is defined in the gantry system and is converted to patient's coordinate system by subtracting 90 degrees. Similarly, for kV-to-DRR registration, we have

$$\begin{cases} q_{KV} = dz \\ p_{KV} = -dx \cdot \sin(G_{KV} - 90) + dy \cdot \cos(G_{KV} - 90) \end{cases} \tag{2}$$

Note that $G_{KV} = G_{MV} - 90$ in gantry system. Then the motion in patient system is calculated as

$$\begin{cases} dx = p_{MV} \cdot \cos G_{MV} + p_{KV} \cdot \sin G_{MV} \\ dy = p_{MV} \cdot \sin G_{MV} - p_{KV} \cdot \cos G_{MV} \\ dz = \dfrac{q_{MV} + q_{KV}}{2} \end{cases} \tag{3}$$

The entire procedure is summarized in the flowchart in Figure 4.

2.5. Study Design

A phantom study was designed to quantify the accuracy of motion tracking. The LUNGMAN phantom was placed on the couch and aligned to the planning position using a cone beam CT scan. High resolution DRR templates were then calculated using the same cone beam CT acquisition. During beam delivery, the MV and KV images were acquired for the nine MV beam angles (180, 160, 140, 120, 100, 260, 240, 220 and 200 degrees) and the corresponding KV angles (90, 70, 50, 30, 10, 170, 150, 130, 110 degrees). The phantom was then shifted by 2 mm in 1) the longitudinal direction only, 2) the lateral direction only, 3) the vertical direction only, and 4) all three directions, respectively, to simulate patient motions after the initial setup. The acquired MV and KV images were retrospectively analyzed using DRR template matching to calculate 3D shifts, and the errors were analyzed. For comparison, motions detected with a single kV image or a single MV image were also analyzed.

In addition to the phantom study, two patients receiving paraspinal SBRT were retrospectively investigated under an ongoing IRB-approved clinical protocol. The first patient was treated to T8-T9 vertebral bodies, where the diaphragm could bring in uncertainties for registration. For this case, the tracking results using both manual registration and automatic mutual information-based registration were compared. The second patient was treated to L3-L5 vertebral bodies, where MV and kV image quality might be compromised by thick patient body. This dataset was also analyzed to demonstrate the potential impact of time window width for creating synthetic MV images. Both were planned with ECHO using the standard 9-fields template (same gantry angles as in the phantom study) with 6xFFF beams. The prescribed doses were both 2700cGy in three fractions. In addition, two CBCT scans were acquired for each patient, one before the

Author Manuscript Author Manuscript Author Manuscript Author Manuscript

treatment for the patient setup, and the other at the end of the treatment for validating the final motion.

3. RESULTS

3.1. Phantom Study

Figure 5 shows an example of a simultaneous MV-kV image pair used for motion tracking. The synthetic MV image and the triggered on-treatment kV image were obtained at a gantry angle of 180 degrees (kV source was at 90 degrees counterclockwise from the MV source). The synthetic MV image contained 200 continuous frames, with a window interval of 18 seconds. The contrast-to-noise ratio (CNR) around vertebral body edges is generally 2.5 – 3.8 in the synthetic MV image and 3.2 – 5.5 in the KV image.

The treatment plan was delivered to the phantom for the following five scenarios: no shift, 2 mm shift in one of the longitudinal, lateral and vertical directions, and 2 mm shift in all three directions. As an example, Figure 6 demonstrates the detected 3D shifts for all nine beams for the scenario of 2mm lateral shift in the temporal order of delivery. Table 1 summarizes the detected shifts for all the five scenarios in terms of average shift and standard deviation in each direction. The errors between ground truth (actual shift) and the mean values of detected shifts (over nine beams) are listed as well, which were all less than 0.15mm. All standard deviations (over nine beams) are within 0.15mm. It is estimated that the uncertainty of tracking error should be less than 0.30mm, which includes 0.15mm for the error of mean and 0.15mm for the standard deviation.

As a comparison to simultaneous MV-kV imaging, it is also meaningful to see the motion detection accuracy using just the kV or MV imaging alone. As an example, Figure 7 demonstrates the results for the case of 2 mm lateral shift. With the coordinate system defined in Figure 3, the q axes of both MV and KV panels are parallel to the couch's longitudinal direction, and thus q values represent the longitudinal shifts of the phantom for all gantry angles. The direction of p axes, however, changes with gantry angles, and thus p shifts are not directly related to shifts in the coordinates of the couch. Therefore, detected shifts in p direction are less meaningful for adjusting couch position.

3.2 Patient Study

The first patient was treated at T8-T9 vertebral bodies. Figure 8 shows example images including (a) the synthetic MV image at gantry angle of 180 degree, (b) the kV image at kV beam angle of 90 degree, and (c) and (d) the high-resolution bone-only DRR templates at their respective angles. The synthetic MV images were calculated using the first 300 raw MV frames of each beam. Note that the diaphragm was visible and overlapping with the spine targets at several imaging angles, which could bring errors in MI-based registration due to significant respiratory motion. To minimize such an impact, bone-only DRRs were created where the diaphragm was eliminated. To ensure the accuracy of image registrations, manual matching was also performed, and the results are shown (solid curves) in Figure 9 together with MI-based registration results (dashed curves). MI-based results were in good agreement with the manual results in the three directions. Their differences, calculated as

Author Manuscript Author Manuscript Author Manuscript Author Manuscript

absolute errors, are summarized in Table 2. For all three directions, the average difference is less than 0.18mm, and the majority (75% percentile) of the differences are smaller than 0.27mm. Since the patient underwent one CBCT for initial setup and a second CBCT right after beam delivery, the two CBCTs can be compared to show the final motions after treatment, which were (shifts only): −0.4mm laterally, −0.6mm vertically and 0.7mm longitudinally. This agreed well with MV-kV tracking results using manual registration at the last beam angle (200 degrees), which were 0.0mm, −0.2mm and 0.6mm, respectively.

The second patient was treated at L3-L5 vertebral bodies. Figures 10 shows examples of MV, kV and DRR images, and Figure 11 shows 3D shifts calculated based on the MV-kV images. The second CBCT confirmed the motion was 0.7mm laterally, −0.3mm vertically and −0.6mm longitudinally. This agreed well with detected shifts using MV-kV tracking at the last beam (200 degrees), which were 0.4mm, −0.1mm and −0.5mm, respectively.

4. DISCUSSION

The proposed MV-kV motion tracking technique was quantitatively evaluated through a phantom study and further validated with two patient studies. The detected 3D shifts agreed well with the physical setup with an uncertainty of less than 0.3mm in all phantom studies. The patient study demonstrated that the proposed MV-kV motion tracking approach worked as expected for T-spine and L-spine treatment in a clinical setting.

MV-kV images provide complementary tracking information from orthogonal views, which is especially favorable over a single image system if one of the images shows inferior quality. For example, certain lateral kV images might show inferior image quality for large patients, however, the simultaneous MV images from the anterior-posterior direction usually show good image quality due to shorter x-ray path through the patient.

The MV-kV formulism was constructed based on the assumption of a perfect geometry, i.e. the mechanical isocenter is aligned perfectly with the kV imaging isocenter and the MV radiation isocenter. In reality, geometrical errors are introduced into the system by several sources, of which the main source is gantry sagging. For the linear accelerator systems used for this study, gantry sagging is about 0.22mm according to the vendors routine Preventive Maintenance Inspections (PMI). At this magnitude, gantry sagging may bring in some errors at certain gantry angles. This effect is already included in the uncertainty of 0.3mm in the phantom study.

The temporal resolution of tracking is basically determined by the length of the time window used for calculating synthetic MV images, and this time period can be shortened with the trade-off of increased registration uncertainties. Synthetic MV images can be calculated using raw MV frames acquired within different time windows (Li *et al* 2021) and they produce different regions of a patient's anatomy with different MLC aperture sizes and shapes. As the example shown in Figure 12, the synthetic MV images were calculated for the beam at 100° gantry angle, where a total of 402 raw MV frames were collected. Figure 12(a) shows the synthetic MV image by combining all 402 raw MV frames, and (b) and (c) were obtained by combining 200 raw MV frames (frames 1–200 and 201–400), both

Author Manuscript Author Manuscript Author Manuscript Author Manuscript

of which showed sufficient FOV and decent anatomy contrast. Figures 12(d), 12(e) and 12(f) were selected from 100-frame combinations, using frames 1–100, 101–200 and 201–300, respectively. The FOVs were smaller and anatomies that can be useful for registration were limited. Figures 12(g), 12(h) and 12(i) were selected from 50-frame combinations (frames 1–50, 101–150 and 301–350), where useful anatomies shown in MLC apertures are very limited, thereby causing more uncertainties in MV-to-DRR registration. Deep learning-based rigid image registration approaches could be a helpful in automatically identifying meaningful image features and improving detection sensitivity and accuracy even with a smaller MV aperture, which are being investigated by our group. Neural network models for optical flow estimation approaches (Teo *et al* 2019 and Shi *et al* 2021) are a potential direction for improving the accuracy and efficiency of automatic motion detection.

The proposed MV-kV motion tracking approach for spinal treatment is not limited to IMRT beams at static gantry angles, and it can be expanded to volume modulated arc therapy (VMAT) plans with some modifications. As previously reported, the MV-kV technique has been used for motion tracking in prostate SBRT (Happersett *et al* 2019, Hunt *et al* 2016, Crotteau *et al* 2022). In this technique, when KV is triggered, MLC apertures are open wider to expose at least one fiducial and the dose rate is reduced to acquire MV images (Happersett *et al* 2019). This idea can be adapted for VMAT spinal treatment in the future.

It should be noted that only translational motions were considered in this study. 2D-2D registration tracks translational motion very well, and in many cases, it can give good estimates to correct for rotational motions (pitch, roll and yaw) by applying translational shifts only, as long as the center of rotational motion is away from PTV (which is often the case). This has been reported in MV-KV imaging-based motion tracking for prostate SBRT (Zhang *et al* 2016, Gorovets *et al* 2020, Happersett *et al* 2019, Hunt *et al* 2016, Crotteau *et al* 2022). However, in some cases, it is the intrinsic limitation that a 2D-2D registration together with translational shift cannot correct motion with rotational motion. 2D-3D registration algorithm can be applied to generate six-degree of freedom shifts (Furtado *et al* 2014, Munbodh *et al* 2014, Kuo *et al* 2020). However, for the task of motion detection (rather than realignment), 2D-2D registration is sufficient (Fan *et al* 2021).

While manual registration was used in this study as the golden standard, mutual information-based registration was also tested for patients to demonstrate the feasibility of automated MV-kV tracking in real clinical settings. MI-based registration is readily available for kV-to-DRR registration, and it generally worked well for MV-to-DRR registration if an appropriate ROI is defined. Our group is also working on novel methods to enhance kV and MV images and to segment bones out of KV and MV images to achieve more accurate and reliable automatic registration (He *et al* 2022). The manual matching results were also validated by the second CBCT scan, which further confirmed the feasibility of using our proposed MV-kV method in a clinic setting.

To implement the MV-KV tracking technique in clinical settings, there are some challenges that should be noted. A standalone workstation should be configured to efficiently perform high-resolution CBCT reconstruction and calculate DRR templates. The quality of MV and KV images and visibility of relevant anatomies vary across patients and view angles,

Author Manuscript Author Manuscript Author Manuscript Author Manuscript

which might produce uncertainties and failures in registration. These should be evaluated through pilot patient studies to determine action levels. The patient should be re-imaged and repositioned if motion exceeds thresholds.

5. CONCLUSIONS

The MV-KV imaging-based markerless motion tracking technique for paraspinal SBRT treatments was validated through a feasibility study. This technique can be readily integrated with our current clinical workflow, and it provides the radiation therapists with quantitative information of patient motion during beam delivery. This research is a step forward toward more effective motion tracking and accurate treatment delivery for spine SBRT.

ACKNOWLEDGEMENTS

Memorial Sloan Kettering Cancer Center has a research agreement with Varian Medical Systems. This research was partially supported by the NIH/NCI Cancer Center Support Grant/Core Grant (P30 CA008748).

References

Bertholet J, Knopf A, Eiben B, et al. 2019 Real-time intrafraction motion monitoring in external beam radiotherapy Phys. Med. Biol. 64(15) 15TR01

Bryant J, Rottmann J, Lewis J, Mishra P, Keall P and Berbeco R 2014 Registration of clinical volumes to beams-eye-view images for real-time tracking Med. Phys. 41(12) 121703 [PubMed: 25471950]

Crotteau K, Lu W, Berry S, Happersett L, Burleson S and Cai W 2022 Retrospective analysis of MV-kV imaging-based fiducial tracking in prostate SBRT treatment J. Appl. Clin. Med. Phys. 23(6) e13593 [PubMed: 35338574]

De Bruin K, Dahele M, Mostafavi H, Slotman Band Verbakel W 2021 Markerless real-time 3-demensional kV tracking of lung tumors during free breathing stereotactic radiation therapy Adv. Radiat. Oncol. 6(4) 100705 [PubMed: 34113742]

Fan Q, Pham H, Zhang P, Li X, Li T 2022 Evaluation of a proprietary software application for motion monitoring during stereotactic paraspinal treatment J. Appl. Clin. Med. Phys. 23(6) e13594 [PubMed: 35338583]

Furtado H, Steiner E, Stock M, Georg D, Birkfellner W 2014 Real-time intensity based 2D/3D registration using kV-MV image pairs for tumor motion tracking in image guided radiotherapy Proc. SPIE 9034 90340H

Furweger C, Drexler C, Kufeld M, Muacevi A and Wowra B 2011 Advances in fiducial-free image-guidance for spinal radiosurgery with CyberKnife - a phantom study J. Appl. Clin. Med. Phys. 12(2) 20–28

Gorovets D, Burleson S, Jacobs L, et al. 2020 Prostate SBRT With Intrafraction Motion Management Using a Novel Linear Accelerator-Based MV-kV Imaging Method Pract. Radiat. Oncology. 10(5) e388–e396

Graeper G, Cetnar A, Ayan A and Weldon M 2021 Interpretation of intrafraction motion review data and method for verification J. Appl. Clin. Med. Phys. 22(11) 196–202

Greco C, Pares O, Pimentel N, Moser E, Louro V, Morales X, Salas B and Fuks Z 2015 Spinal metastases: From conventional fractionated radiotherapy to single-dose SBRT Reports of Practical Oncology & Radiotherapy 20(6) 454–463 [PubMed: 26696786]

Gurney-Champion O, Dahele M, Mostafavi H, Slotman B and Verbakel W 2013 Digital tomosynthesis for verifying spine position during radiotherapy: a phantom study Phys. Med. Biol. 58(16) 5717–5733 [PubMed: 23902917]

Hall W, Stapleford L, Hadjipanayis C, Curran W, Crocker I and Shu H 2011 Stereotactic body radiosurgery for Spinal Metastatic Disease: an evidence-based review Int. J. Surg. Onc. 2011: 979214

Author Manuscript Author Manuscript Author Manuscript Author Manuscript

Happersett L, Wang P, Zhang P, et al. 2019 Developing a MLC modifier program to improve fiducial detection for MV/kV imaging during hypofractionated prostate volumetric modulated arc therapy J. Appl. Clin. Med. Phys. 20(6) 120–124

Hazelaar C, Verbakel W, Mostafavi H, van der Weide L, Slotman B and Dahele M 2018 First experience with markerless online 3D spine position monitoring during SBRT delivery using a conventional LINAC Int. J. Radiat. Oncol. Biol. Phys. 101(5) 1253–1258 [PubMed: 29908789]

He X, Cai W, Li F, Fan Q, Zhang P, Cuaron J, Cerviño L, Li X and Li T 2021 Decompose kV projection using neural network for improved motion tracking in paraspinal SBRT Med. Phys. 48(12) 7590–7601 [PubMed: 34655442]

Ho A, Fu D, Hancock S, et al. 2007 A study of the accuracy of CyberKnife spinal radiosurgery using skeletal structure tracking Neurosurgery 60(2) ONS147–156 [PubMed: 17297377]

Hunt M, Sonnick M, Pham H, et al. 2016 Simultaneous MV-kV imaging for intrafractional motion management during volumetric modulated arc therapy delivery J. Appl. Clin. Med. Phys. 17(2) 473–486 [PubMed: 27074467]

Jiang S, Lu Y, Li H, Hartley R 2021 Learning optical flow from a few matches CVPR 2021 16592–16600

Jin J, Yin F, Tenn SE, Medin PM and Solberg T 2008 Use of the BrainLAB ExacTrac X-Ray 6D System in Image-Guided Radiotherapy Med. Dosi. 33(2) 124–134

Kaur G, Lehmann J, Greer P and Simpson J 2019 Assessment of the accuracy of truebeam intrafraction motion review (IMR) system for prostate treatment guidance Australas. Phys. Eng. Sci. Med. 42(2) 585–598 [PubMed: 31087231]

Keall P, Nguyen D, O'Brien R, et al. 2018 Review of real-time 3D IGRT on standard-equipped cancer radiotherapy systems: are we at the tipping point for the era of real-time radiotherapy Int. J. Radiat. Oncol. Biol. Phys. 102(4) 922–931 [PubMed: 29784460]

Kim J, Nguyen D, Booth J, et al. 2018a The accuracy and precision of Kilovoltage Intrafraction Monitoring (KIM) six degree-of-freedom prostate motion measurements during patient treatments Radiother. and Oncol. 126(2) 236–243

Kim J, Park Y, Edmunds D, Oh K, Sharp G and Winey B 2018b Kilovoltage projection streaming-based tracking application (KiPSTA): first clinical implementation during spine stereotactic radiation surgery Adv in Radiat. Oncol. 3(4) 682–692

Kuo H, Lovelock M, Li G, Ballangrud A, Wolthuis B, Della-Biancia C, Hunt M and Berry S 2020 A phantom study to evaluate three different registration platform of 3D/3D, 2D/3D, and 3D surface match with 6D alignment for precise image-guided radiotherapy J. Appl. Clin. Med. Phys. 21(12) 188–196

Li T, Li F, Cai W, Zhang P and Li X 2021 Technical Note: Synthetic treatment beam imaging for motion monitoring during spine SBRT treatments - a phantom study Med. Phys. 48(1) 125–131 [PubMed: 33231877]

Mishra P, Li R, Mak R, Rottmann J, Bryant J, Williams C, Berbeco R and Lewis J 2014 An initial study on the estimation of time-varying volumetric treatment images and 3D tumor localization from single MV cine EPID images Med. Phys. 41(8) 081713 [PubMed: 25086523]

Montgomery C and Collins M 2017 An evaluation of the BrainLAB 6D ExacTrac/Novalis Tx system for image-guided intracranial radiotherapy J. Radiother. Pract. 16(3) 326–333

Munbodh R and Moseley D 2014 2D-3D registration for brain radiation therapy using a 3D CBCT and a single limited field-of-view 2D kV radiograph J. Phys. Conf. Ser. 489(1) 012037

Nankali S, Worm E, Hansen R, Weber B, Hoyer M, Zirak 2018 A and Poulsen P Geometric and dosimetric comparison of four intrafraction motion adaption strategies for stereotactic liver radiotherapy Phys. Med. Biol. 63 145010 [PubMed: 29923837]

Roggen T, Bobic M, Givehchi N and Scheib S 2020 Deep learning model for markerless tracking in spinal SBRT Phys. Med. 74 66–73 [PubMed: 32422577]

Rozario T, Chiu T, Chen M, Jia X, Lu W, Bereg S and Mao W 2018 A novel markerless lung tumor-tracking method using treatment MV beam imaging Appl. Sci. 8(12) 2525

Saenz D, Crownover R, Stathakis S and Papanikolaou N 2019 A dosimetric analysis of a spine SBRT specific treatment planning system J. Appl. Clin. Med. Phys. 20(1) 154–159

Author Manuscript Author Manuscript Author Manuscript Author Manuscript

Shieh C, Keall P, Kuncic Z, Huang C, Feain I 2015 Markerless tumor tracking using short kilovoltage imaging arcs for lung image-guided radiotherapy Phys Med. Biol. 60(24) 9437 [PubMed: 26583772]

Teo PT, Guo K, Ahmed B, Alayoubi N, Kehler K, Fontaine G, Sasaki D and Pistorius S 2019 Evaluating a potential technique with local optical flow vectors for automatic organ-at-risk (OAR) intrusion detection and avoidance during radiotherapy Phys. Med. Biol. 64 145008 [PubMed: 31252423]

Van Sornsen de Koste J, Dahele M, Mostafavi H, Sloutsky A, Senan S, Slotman B, Verbakel W 2015 Markerless tracking of small lung tumors for stereotactic radiotherapy Med. Phys. 42(4) 1640–1652 [PubMed: 25832054]

Vellayappan B, Chao S, Foote M, Guckenberger M, Redmond K, Chang E, Mayr N, Sahgal A and Lo S 2018 The evolution and rise of stereotactic body radiotherapy (SBRT) for spinal metastases Expert Review of Anticancer Therapy 18(9) 887–900 [PubMed: 29940802]

Verbakel W, Gurney-Champion O, Slotman B and Dahele M 2015 Sub-millimeter spine position monitoring for stereotactic body radiotherapy using offline digital tomosynthesis Radiother. and Oncol. 115(2) 223–228

Yue Y, Aristophanous M, Rottmann J, Berbeco R 2011 3-D fiducial motion tracking using limited MV projections in arc therapy Med. Phys. 38(6) 3222–3231 [PubMed: 21815397]

Zarepisheh M, Hong L, Zhou Y, Oh J, Mechalakos J, Hunt M, Mageras G, Deasy J 2019 Automated intensity modulated treatment planning: The expedited constrained hierarchical optimization (ECHO) system Med. Phys. 46(7) 2944–2954 [PubMed: 31055858]

Zeng K, Tseng C, Soliman H, Weiss Y, Sahgal A and Myrehaug S 2019 Stereotactic Body Radiotherapy (SBRT) for Oligometastatic Spine Metastases: An Overview Frontiers in Oncology 9 337 [PubMed: 31119099]

Zhang P, Happersett L, Ravindranath B, et al. 2016 Optimizing fiducial visibility on periodically acquired megavoltage and kilovoltage image pairs during prostate volumetric modulated arc therapy Med. Phys. 43(5) 2024 [PubMed: 27147314]

Author Manuscript Author Manuscript Author Manuscript Author Manuscript

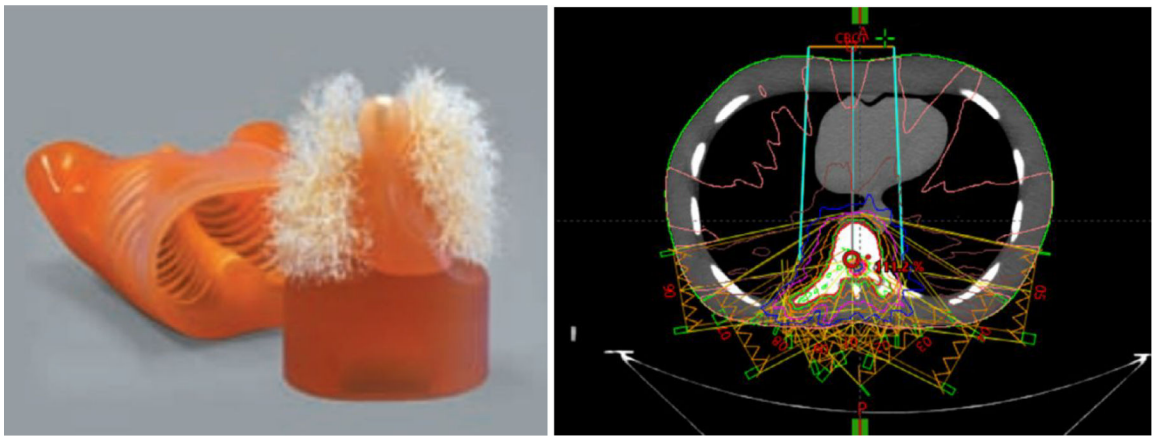

Figure 1.
The anthropomorphic thorax phantom (left) and the field setup of a treatment plan developed using the phantom (right).

Author Manuscript Author Manuscript Author Manuscript Author Manuscript

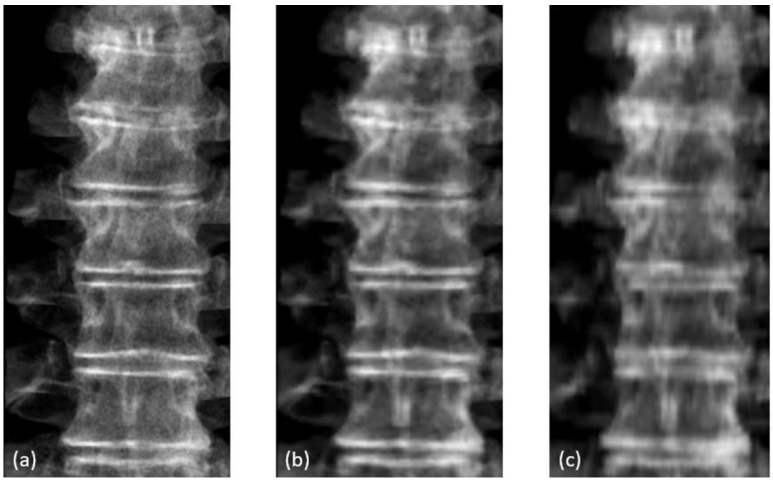

Figure 2.
Comparison of DRRs created from CBCT with different voxel size: (a) 0.243×0.243×0.243 mm^3, (b) 1×1×1 mm^3, and (c) 1×1×2 mm^3.

Author Manuscript Author Manuscript Author Manuscript Author Manuscript

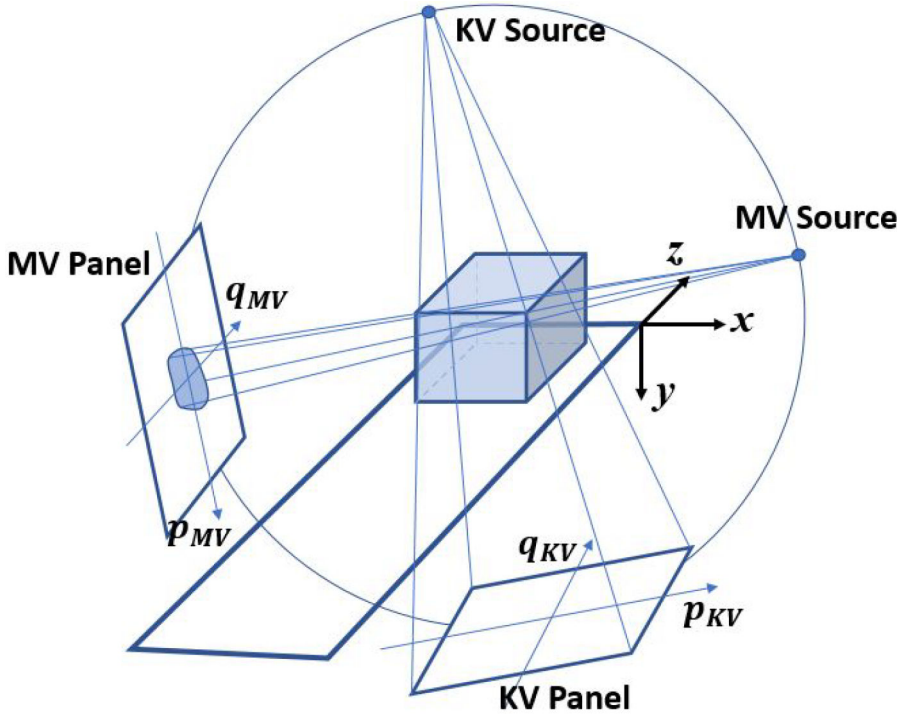

Figure 3.
Geometry of motion tracking with simultaneous MV-kV imaging on a conventional linear accelerator.

Author Manuscript Author Manuscript Author Manuscript Author Manuscript

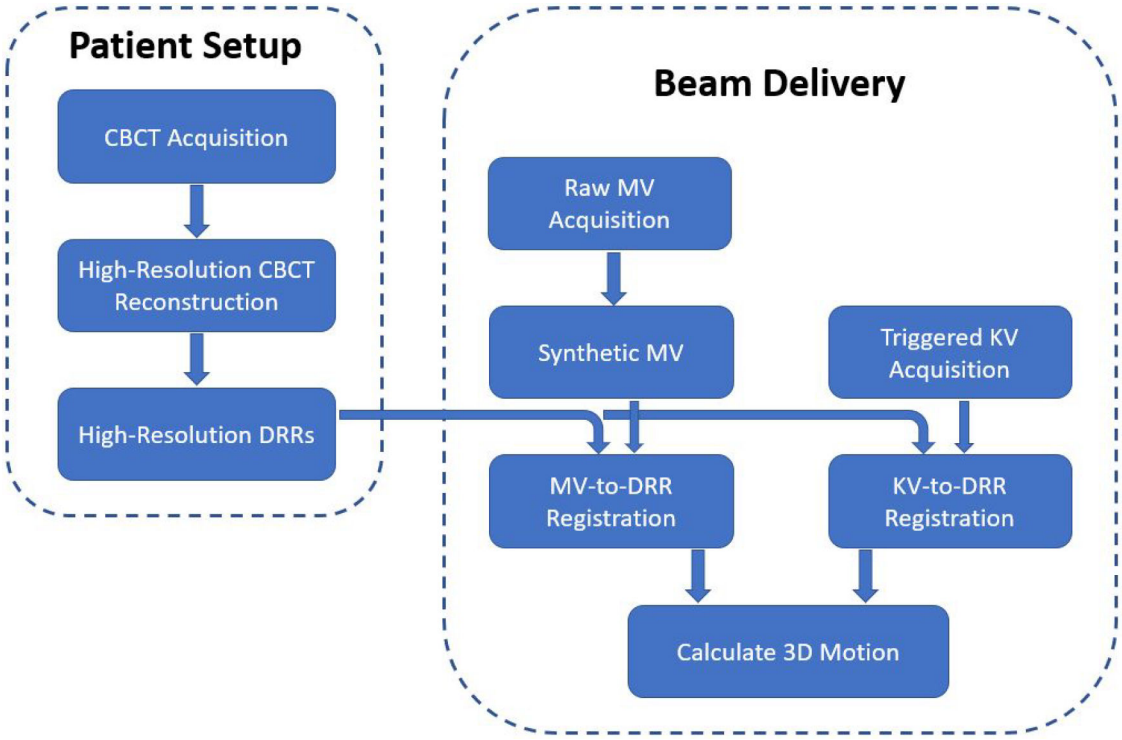

Figure 4.
Flowchart of the proposed approach of motion tracking using orthogonal MV and KV images

Author Manuscript Author Manuscript Author Manuscript Author Manuscript

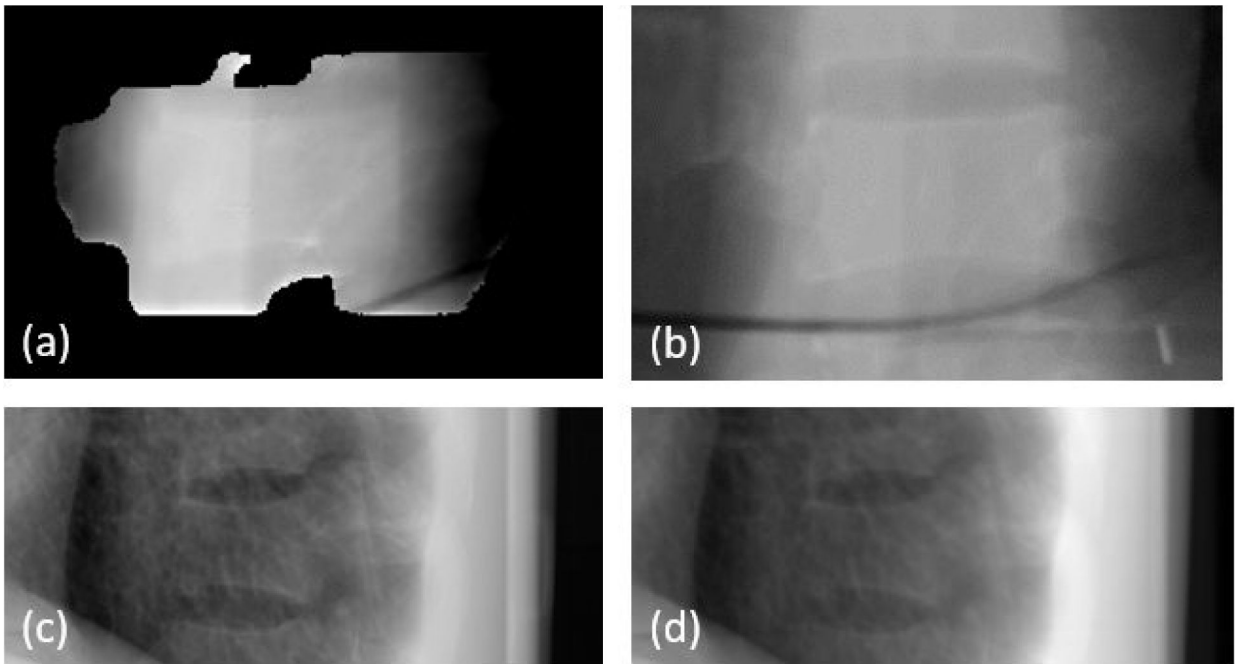

Figure 5.
Example of phantom images: (a) synthetic MV image at gantry angle of 180 degree, (b) DRR at MV angle, (c) kV image at kV angle of 90 degree and (d) DRR at KV angle.

Author Manuscript Author Manuscript Author Manuscript Author Manuscript

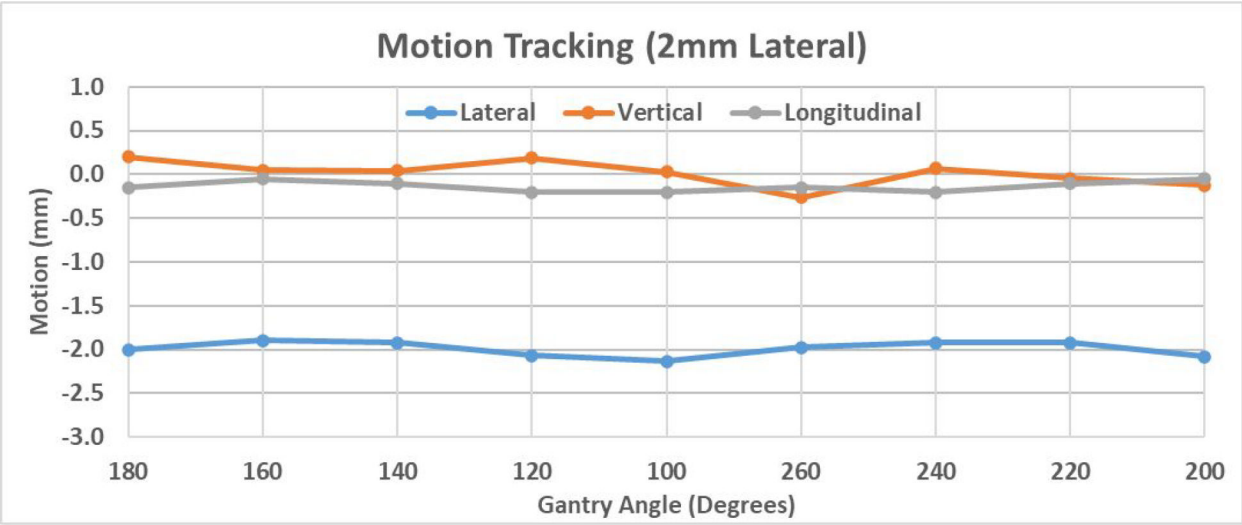

Figure 6.

Demonstration of 3D shift detected by MV-KV approach in the scenario of a 2mm shift in the lateral direction.

Author Manuscript Author Manuscript Author Manuscript Author Manuscript

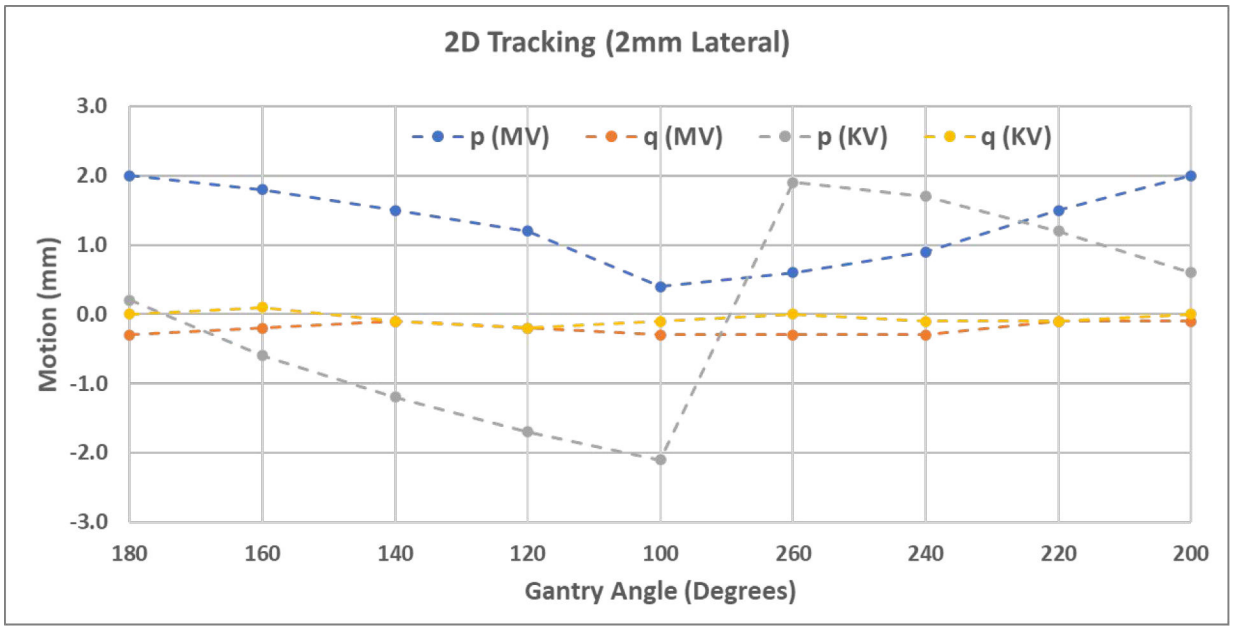

Figure 7.

Shifts detected by single kV or MV images in the detector *p*-*q* plane in the scenario of a 2mm lateral shift.

Author Manuscript Author Manuscript Author Manuscript Author Manuscript

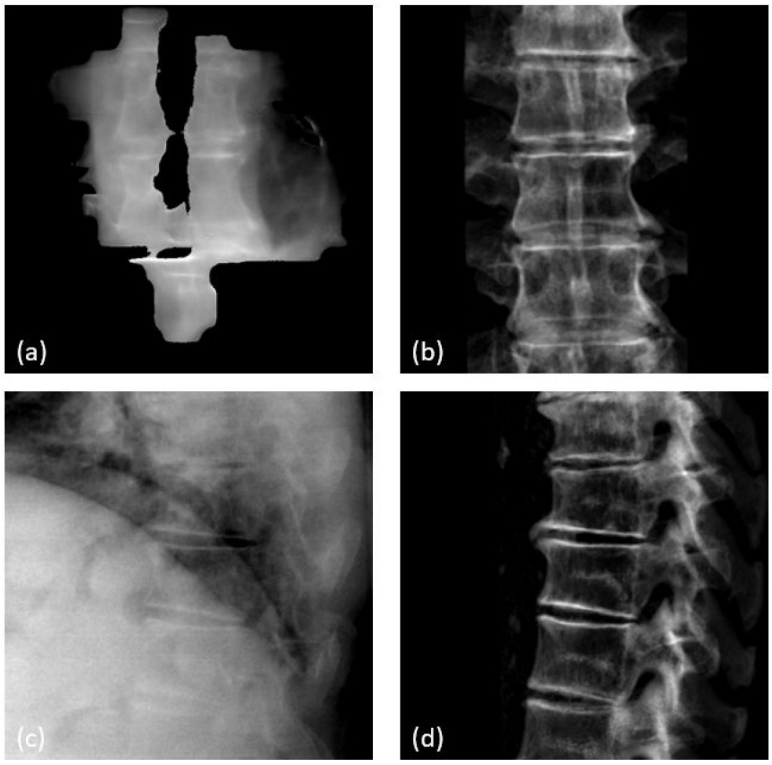

Figure 8.
T-spine patient images: (a) synthetic MV image at gantry angle of 180 degrees, (b) DRR at MV angle, (c) KV image at KV angle of 90 degrees, and (d) DRR at kV angle.

Author Manuscript Author Manuscript Author Manuscript Author Manuscript

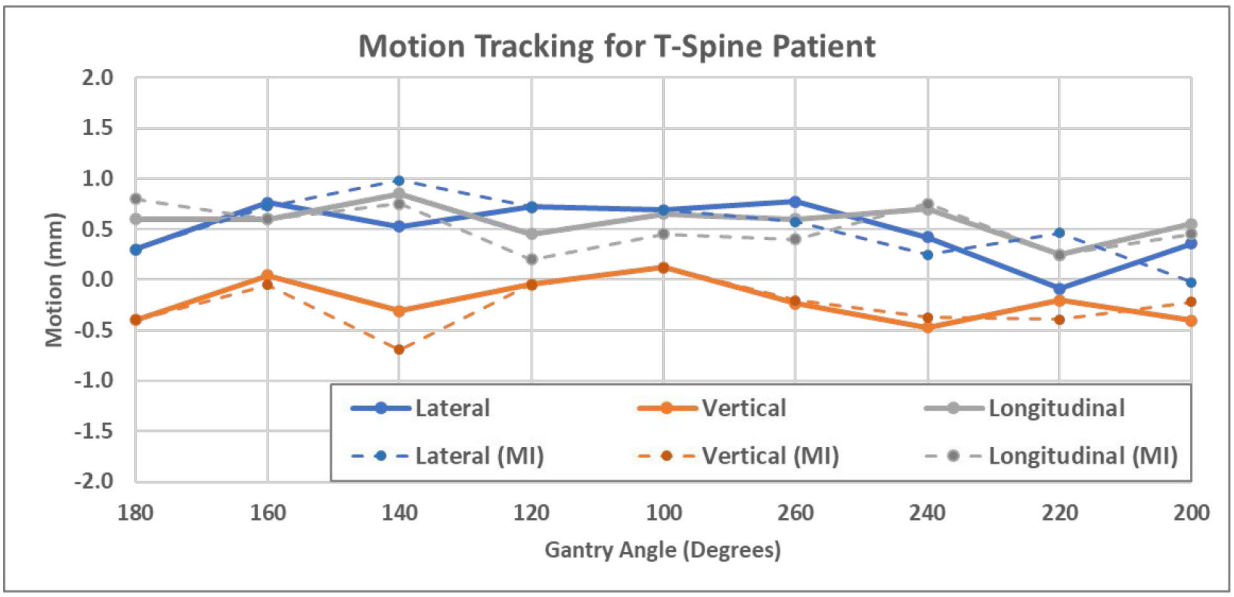

Figure 9.

3D shifts of the T-spine patient calculated using both manual registration (solid) and MI-based registration (dashed).

Author Manuscript Author Manuscript Author Manuscript Author Manuscript

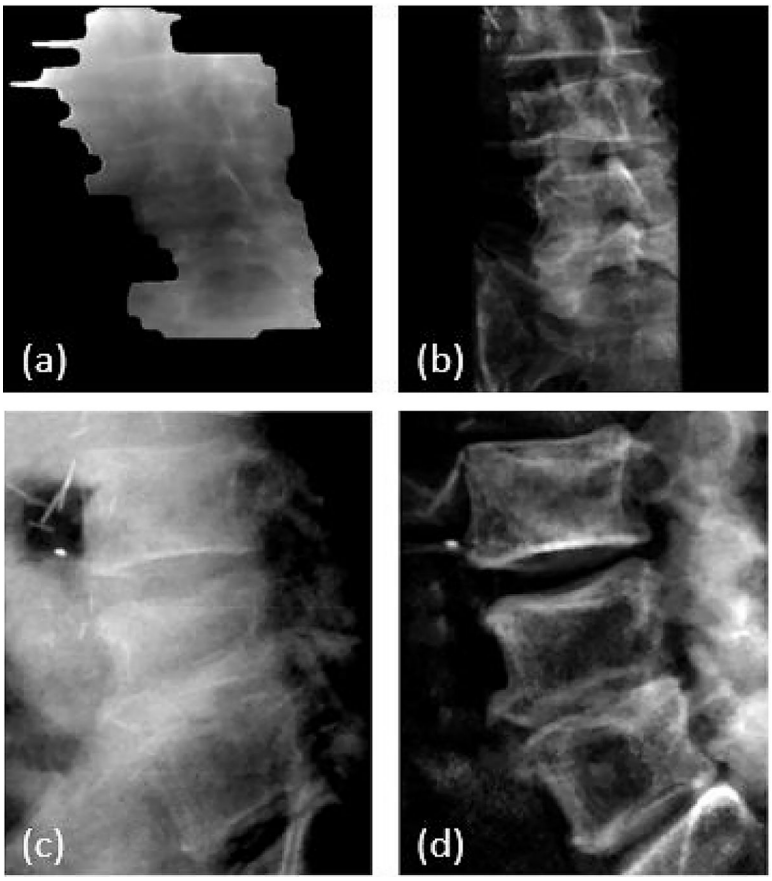

Figure 10.
L-spine patient images: (a) synthetic MV image at gantry angle of 180 degrees, (b) DRR at MV angle, (c) kV image at kV angle of 90 degrees and (d) DRR at kV angle.

Author Manuscript Author Manuscript Author Manuscript Author Manuscript

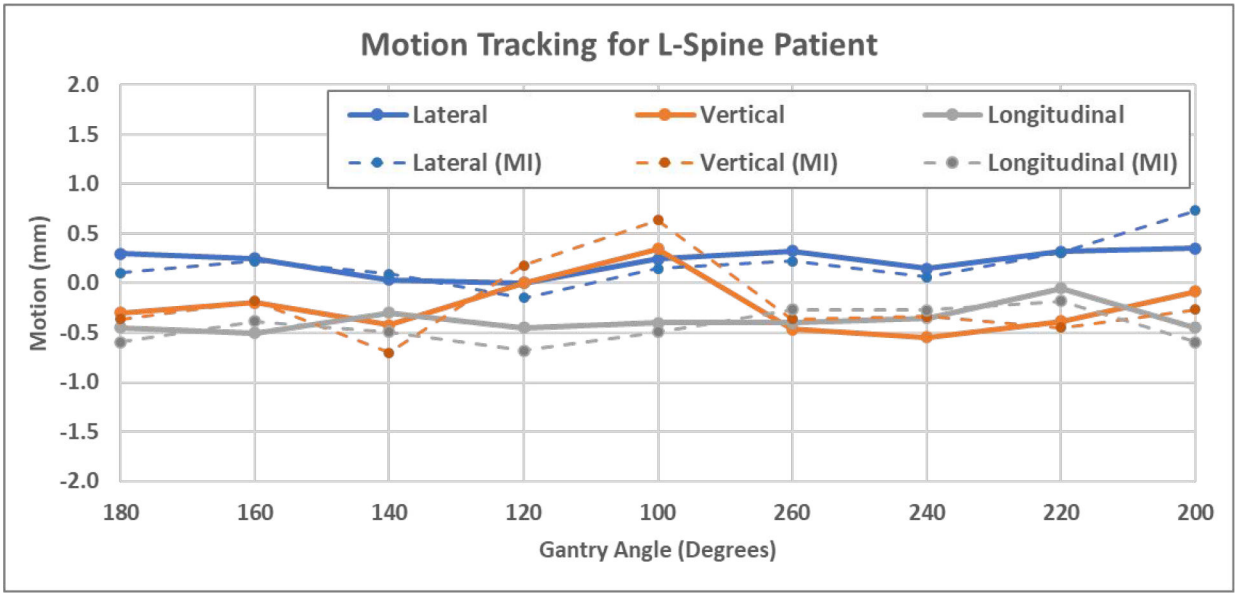

Figure 11.

3D shifts of the L-spine patient calculated using manual registration (solid) and MI-based registration (dashed).

Author Manuscript Author Manuscript Author Manuscript Author Manuscript

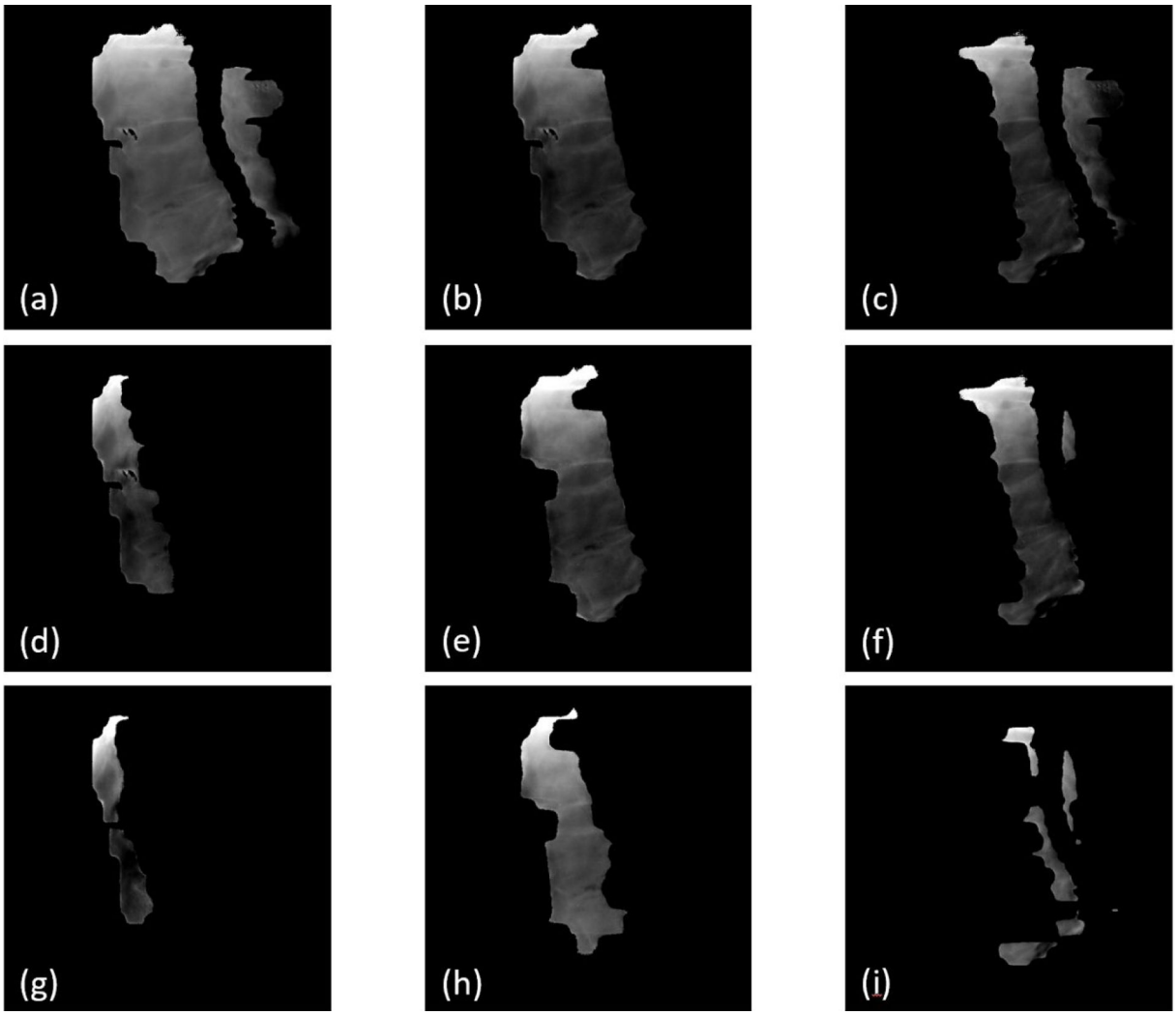

Figure 12.

Synthetic MV images calculated by combining raw MV frames acquired in various time windows. (a) was calculated by combining all 402 raw MV frames; (b) and (c) are 200-frame combinations (frames 1–200 and 201–400, respectively); (d), (e) and (f) are 100-frame combinations (frames 1–100, 101–200 and 201–300), respectively; (g), (h) and (i) are 50-frame combinations (frames 1–50, 101–150 and 301–350, respectively).

Author Manuscript

Author Manuscript

Author Manuscript

Author Manuscript

Table 1.

Summary of detected phantom shifts for the five scenarios

	Lateral		Vertical		Longitudinal	
	Mean (Std) (mm)	**Error (mm)**	**Mean (Std) (mm)**	**Error (mm)**	**Mean (Std) (mm)**	**Error (mm)**
No Shift	0.00 (0.09)	0.00	0.04 (0.06)	0.04	−0.15 (0.07)	−0.15
2mm Lng	0.06 (0.08)	0.06	0.07 (0.13)	0.07	−2.13 (0.08)	−0.13
2mm Vrt	0.05 (0.10)	0.05	−1.92 (0.05)	0.08	−0.12 (0.04)	−0.12
2mm Lat	−1.99 (0.09)	0.01	0.02 (0.14)	0.02	−0.13 (0.06)	−0.13
2mm All	−2.04 (0.10)	−0.04	−1.94 (0.11)	0.06	−2.01 (0.10)	−0.01

Author Manuscript

Author Manuscript

Author Manuscript

Author Manuscript

Table 2.

Summary of absolute errors between manual results and MI-based results for patient studies

	Mean (mm)	STD (mm)	Max (mm)	Quart-75% (mm)
T-spine patient				
Lateral	0.16	0.19	0.61	0.18
Vertical	0.18	0.18	0.51	0.27
Longitudinal	0.17	0.20	0.65	0.20
L-spine patient				
Lateral	0.12	0.11	0.28	0.15
Vertical	0.15	0.10	0.29	0.21
Longitudinal	0.14	0.05	0.23	0.15